Applied Catalysis B: Environmental 198 (2016) 411–419

Contents lists available at ScienceDirect

Applied Catalysis B: Environmental

journal homepage: www.elsevier.com/locate/apcatb

# $NO_2$ adsorption mechanism on $TiO_2$: An *in-situ* transmission infrared spectroscopy study

L. Sivachandiran[a,b,c,*], F. Thevenet[a,b], A. Rousseau[c], D. Bianchi[d]

[a] Mines Douai, SAGE, F-59508 Douai, France
[b] Université de Lille, F-59000 Lille, France
[c] Laboratoire de Physique des Plasmas, École Polytechnique, UPMC, Université Paris Sud 11, CNRS Palaiseau, France
[d] IRCELYON Université Claude Bernard Lyon 1, Bat Chevreul, UMR CNRS 5658, F-69100 Villeurbanne, France

ARTICLE INFO

*Article history:*
Received 11 April 2016
Received in revised form 25 May 2016
Accepted 27 May 2016
Available online 2 June 2016

*Keywords:*
$TiO_2$
$NO_2$
Adsorption
Monodentate $NO_3^-$
Bidentate $NO_3^-$

ABSTRACT

The adsorption of $NO_2$ on oxidized $TiO_2$ surface, under dark condition at 296 K, has been investigated by *in-situ* transmission Fourier Transform Infrared Spectroscopy (trans-FTIR) as a function of time. It enabled the determination of detailed $NO_2$ reactive adsorption mechanisms on $TiO_2$. It was evidenced that, as soon as $NO_2$ molecules adsorb on $TiO_2$ surface it dimerize to adsorbed $N_2O_4$ species. The strongly adsorbed $N_2O_4$ undergoes intramolecular disproportionation reaction and produces: (i) weakly adsorbed monodentate nitrate (m-$NO_3^-$) species and, (ii) highly reactive $NO^+$ and/or $N_2O_3$ species on $Ti^{4+}$ sites and $O^{2-}$ sites, respectively. The $NO^+$ species reacts with surface lattice oxygen ($O^{2-}$) and produces more stable $NO_2^-$ on $Ti^{4+}$ sites. Then, the $NO_2^-$ undergoes intermolecular disproportionation reaction with another strongly adsorbed $N_2O_4$ molecule and produces strongly adsorbed bidentate nitrate (b-$NO_3^-$) species on $Ti^{4+}$ sites and releases NO in the gas phase. It was also noticed that, as adsorption time increases, the weakly adsorbed m-$NO_3^-$ species are converted into strongly adsorbed b-$NO_3^-$ species. The intramolecular disproportionation reaction rate depends on $NO_2$ partial pressure, whereas the intermolecular disproportionation reaction rate depends on the coverage of $NO_2^-$ species and the number of available $Ti^{4+}$ sites. This mechanism is assessed for different $NO_2$ partial pressures ranging from 25 to 100 Pa. This study reveals that the configuration and the amount of the N-containing species on activated $TiO_2$ surface depend on the $NO_2$ concentration and the contact time.



## 1. Introduction

Tropospheric Emission Monitoring Internet Service (TEMIS) [1] reports that most of the $NO_2$ emission originates from the European Union and China. The U.S. Environmental Protection Agency (EPA) regulates only nitrogen dioxide ($NO_2$) as a surrogate for $NO_X$, because it is the most prevalent form of $NO_X$ in the atmosphere generated by anthropogenic activities [2]. $NO_2$ is not only an important air pollutant by itself, but it is also a key reactant in the atmosphere to form ozone ($O_3$) through series of reactions with volatile organic compounds (VOCs) [3] and acid rain.

$NO_2$ is produced in combustion processes under lean, *i.e.* oxygen-rich conditions. Emerging technologies favor the formation of $NO_2$ instead of NO during the combustion of fuels because the high reactivity of $NO_2$ makes easier subsequent DeNOx operations [4,5]. In DeNO$_X$ process, owing to its acidic property, thermal and mechanical stability, $\gamma$-$Al_2O_3$ is a widely used support [6]. However, new support materials are also studied either in their pure form or in mixture with other metal-oxides [7]. In this regards $TiO_2$ has been intensively studied due to its better sulfur tolerance [8] and controlled surface dispersion of barium oxide (BaO) [9] as compared to $\gamma$-$Al_2O_3$.

In particular, the most important step in DeNO$_X$ process is the adsorption of $NO_2$ on supporting materials. In spite of stability, $NO_2$ molecule strongly adsorbs on metal centers due to high electron affinity [10] (2.3 eV). It is demonstrated that metal oxides are very efficient as sorbents or catalysts for trapping and/or converting $NO_2$ and other $NO_X$ species [11–14]. It is reported that depending on the $NO_X$ concentration and adsorption time, there may be variation in thermal regeneration temperature and time [15]. Therefore, it

* Corresponding author at: GREMI, CNRS-Université d'Orléans, 45067 Orléans, France.
*E-mail address:* sivachandiran.loganathan@univ-orleans.fr (L. Sivachandiran).

http://dx.doi.org/10.1016/j.apcatb.2016.05.065
0926-3373/

is necessary to understand the nature of the adsorbed species on metal oxide surface to optimize the $NO_X$ removal process.

Ramis et al. examined the $NO_2$ adsorption on $TiO_2$ surface at room temperature and evidenced that $NO_2$ adsorbs on $Ti^{4+}$ sites through O, N, or a combination of both [16,17]. Hadjiivanov et al. [18] and Dalton et al. [19] demonstrated the $NO_2$ adsorption on anatase surface and showed that isolated OH-groups on $TiO_2$ surface react with $NO_2$ to produce adsorbed $NO_3^-$ and water, on $TiO_2$ surface, and NO in the gas phase. In addition, authors have also reported that α and β- Lewis sites on $TiO_2$ surface respectively produce mono and bidentate $NO_3^-$ species. This work is not in complete agreement with other approaches based on accurate gas phase analyses [15]. Indeed, Sivachandiran et al. [15] evidenced that, under dark condition, the nature of species adsorbed on $TiO_2$ surface highly depends on: (i) the $NO_2$ concentration and (ii) the duration of adsorption. The proposed mechanism by Sivachandiran et al. [15] is summarized in Eq. (1) to Eq. (3).

$$2NO_{2\,(ads)} \leftrightarrow NO_{3\,(ads)}^- + NO^+_{\,(ads)} \quad (1)$$

$$NO^+_{\,(ads)} + O^{2-}(TiO_{2surface\ \ lattice}) \leftrightarrow NO_{2\,(ads)}^- \quad (2)$$

Surface coverage $\left(NO_{2\,(ads)}^- + NO_{3\,(ads)}^-\right) > 0.2$ then:

$$NO_{2\,(ads)}^- + NO_{2\,(ads)} \leftrightarrow NO_{3\,(ads)}^- + NO_{(g)} \quad (3)$$

Therefore, the global $NO_2$ adsorption stoichiometry equation can be written by summing up Eq. (1) to Eq. (3) as denoted in Eq. (4):

$$3NO_{2\,(ads)} + O^{2-}(TiO_{2surface\ \ lattice}) \leftrightarrow 2NO_{3\,(ads)}^- + NO_{(g)} \quad (4)$$

According to Eq. (4), three $NO_2$ molecules are involved to produce one NO in the gas phase and two $NO_3^-$ species adsorbed on $TiO_2$ surface. In one hand, as reported in Eq. (1), the first $NO_3^-$ species is produced by disproportionation reaction between two adsorbed $NO_2$ species. Then, as reported in Eq. (3), the second $NO_3^-$ is produced by disproportionation reaction between the produced intermediate species $NO_2^-$ and the molecularly adsorbed $NO_2$. Thus, it can be proposed that, these two $NO_3^-$ species could be different regarding their adsorption modes. Indeed, it was noticed that [15], during temperature programmed desorption (TPD), the adsorbed $NO_3^-$ species are desorbed in two distinct peaks. These findings means that, the desorption energies of $NO_3^-$ species produced in Eq. (1) and in Eq. (3) are different. In addition to that, with increasing the adsorption time, the first $NO_3^-$ desorption peak disappears. Thus, it can be suggested that, as the time progress the weakly adsorbed $NO_3^-$ is converted into strongly adsorbed $NO_3^-$ species. To assess these hypotheses and to follow the evolution of other adsorbed species, it is necessary to monitor the $TiO_2$ surface directly and continuously.

In this study, $NO_2$ adsorption mechanism has been investigated on $TiO_2$ surface, under dark condition at 296 K. The *in-situ* Transmission Fourier Transform Infrared Spectroscopy (trans-FTIR) was used to investigate the adsorbed species on $TiO_2$ surface before and after $NO_2$ adsorption experiments. The evolution of adsorbed species on $TiO_2$ surface is continuously monitored for various $NO_2$ partial pressures like 25 and 100 Pa as a function of time in order to propose new insights regarding reactive adsorption mechanism of $NO_2$ on $TiO_2$.

## 2. Experimental description

Fig. 1 gives a general overview of the experimental and analytical setup. This experimental setup is adapted from the setup used and reported by Arsac et al. [20] for photocatalytic studies. In brief, the main body of the reactor consists of a Pyrex tube characterized by 40 mm of outer diameter, 35 mm of inner diameter and 2.5 mm of wall thickness. As shown in Fig. 1, four different parts can be distinguished in this experimental setup: (1) Gas stream preparation

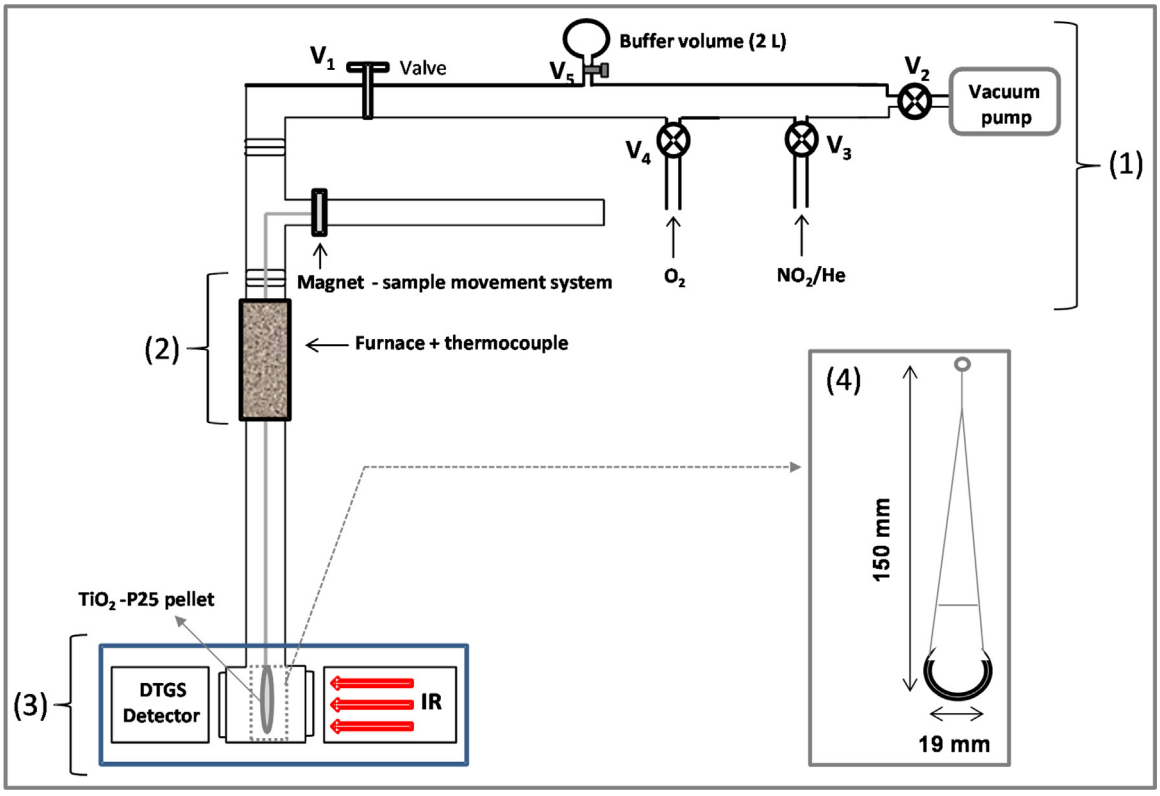


**Fig. 1.** General schematic of the experimental setup.

and pumping, (2) Furnace for thermal pretreatment, (3) trans-FTIR, and (4) $TiO_2$ sample holder.

### 2.1. $TiO_2$ sample preparation, gas stream introduction

The $TiO_2$ sample is prepared by compressing 70 mg of $TiO_2$-P25 Degussa powder with $5 \times 10^4$ Pa pressure. The obtained pellet is a disc of 18 mm diameter. Then the sample is placed inside the quartz sample holder (4), Fig. 1, by removing the part (2). As presented in insert part (4) of Fig. 1, the length of the sample holder is 150 mm. One end of the sample holder is connected to the magnetic movement system using tungsten wire, while the other end is specially designed with a round shape of 19 mm inner diameter to hold the $TiO_2$ disc. The reactor is pumped down by opening the valve $V_2$ connected to a vacuum pump. Thus, a minimum total pressure of 0.5 Pa can be reached in the reactor.

The valves $V_3$ and $V_4$ are respectively used to introduce 1% $NO_2$/He, and pure $O_2$. The total volume of the reactor has been evaluated by volumetric method using the buffer volume connected through the valve $V_5$. The determined volume is $2 \pm 0.1$ L. Before adsorption, it is necessary to purge the valves and the upstream pipe lines connected to the gas cylinders to avoid the $TiO_2$ sample contamination. The valve $V_1$ is used to isolate the part (1) from other parts of the reactor, and vacuum pump is used to purge the sample port valves ($V_3$, $V_4$) and the upstream line.

### 2.2. $TiO_2$ thermal pretreatment

As can be seen in Fig. 1, the part (2) is made of quartz tube and covered with a removable furnace (Winkler, WRW00110). The furnace is used for sample pretreatment performed before any experiment. The sample temperature can be increased to 700 K and the temperature is monitored using K-type thermocouple placed inside the furnace. On the top of the part (2), a magnetic sample movement system is connected and used to move the quartz sample holder (4), from part (2) to part (3). The sample is carefully moved to the heating part (2). Before thermal treatment the reactor is pumped down to 0.5 Pa total pressure by opening the valve $V_2$. Then, valve $V_2$ is closed and $2 \times 10^4$ Pa of pure $O_2$ are introduced into the reactor by opening the valve $V_4$. Once the pressure reaches the equilibrium, the sample temperature is linearly increased from 296 to 700 K with the heating rate of 1.1 K $s^{-1}$. After 1 h of heating, the reactor is pumped down to 0.5 Pa, again $2 \times 10^4$ Pa of pure $O_2$ are introduced. After 2 h of thermal treatment, the furnace is switched off, the reactor is pumped down to 0.5 Pa and the sample is allowed to cool down to 296 K.

### 2.3. Analytical device: trans-FTIR

In part (3), transmission FTIR cell, so-called trans-FTIR (Brucker IFS-28), is used to characterize species adsorbed on $TiO_2$ sample. The sample surface is characterized before each step of the process. As shown in Fig. 1, the homemade IR cell consists in a Pyrex tube. Both ends of the tube are closed with $CaF_2$ windows characterized by 35 mm diameter and 3 mm thickness. This configuration leads to 80 mm optical path length. Viton O-rings are used to assemble tightly all parts of the IR cell. Further, a Pyrex tube is used to connect the IR cell to the other parts of the reactor. In addition to that, an appropriate system inserted inside the Pyrex tube is used to keep the $TiO_2$ sample in the same position, perpendicular to the IR beam, for all experiments. Finally, the transmitted IR radiations are recorded by DTGS detector at room temperature. The $TiO_2$ sample is continuously scanned from 4000 to 1100 $cm^{-1}$. FTIR spectra are collected and analyzed using OMNIC software with 5 scans per spectrum and 4 $cm^{-1}$ spectral resolution.

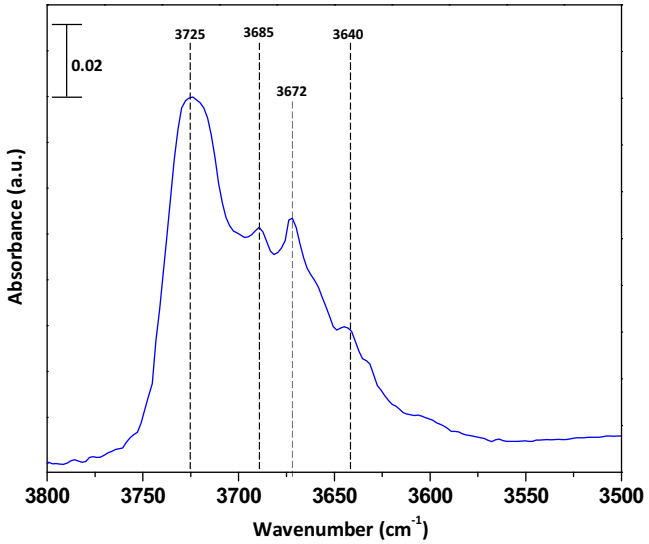


**Fig. 2.** FTIR spectrum of $TiO_2$ pellet recorded at 296 K after thermal pretreatment. $TiO_2$ sample was pretreated under $2 \times 10^4$ Pa total pressure of pure $O_2$ at 700 K for 2 h.

### 2.4. $NO_2$ adsorption experiments

The $NO_2$ adsorption on $TiO_2$ surface has been investigated for two different partial pressures: $25 \pm 2.5$ and $100 \pm 2.5$ Pa. The pressure was monitored using vacuum gauge supplied by Cole-Parmer (EW-07379-22). For $NO_2$ adsorption experiment, the $NO_2$ cylinder is connected to the setup through the valve $V_3$. All the calibrated gas cylinders are provided by Air liquid. During the adsorption experiments, the $TiO_2$ sample is kept in the trans-FTIR cell and the surface is continuously scanned and the adsorbed species are monitored as a function of time.

## 3. Results and discussion

### 3.1. Thermally treated $TiO_2$ surface characterization before $NO_2$ adsorption

Fig. 2 shows the FTIR spectrum of $TiO_2$ surface after the thermal treatment and prior to any $NO_2$ adsorption. After thermal pretreatment, performed under pure $O_2$, the sample has been cooled to 296 K. The gas phase spectrum collected under 0.5 Pa of pure $O_2$ is used as background spectrum. As can be seen in Fig. 2, FTIR spectrum reveals four main IR bands at 3725, 3685, 3672 and 3640 $cm^{-1}$. The bands at 3725 and 3685 $cm^{-1}$ are ascribed to isolated OH groups, and bands at 3672 and 3640 $cm^{-1}$ are assigned to bridged hydroxyl groups [20–23]. The multiplicity of the hydroxyl groups on $TiO_2$-P25 sample is attributed to the presence of variety of $Ti^{4+}$ sites on surface [23].

### 3.2. Temporal profiles of $NO_2$ adsorption on $TiO_2$ under dark condition

For adsorption, $25 \times 10^2$ Pa of 1% $NO_2$ in He, *i.e.* 25 Pa of $NO_2$ partial pressure, are introduced into the reactor. Fig. 3 shows the FTIR spectra of $TiO_2$ exposed to $NO_2$ for different durations. The assignment of the absorption bands of adsorbed species on $TiO_2$ surface is given in Table 1 [16–18,24,25,26,27].

The introduction of $NO_2$ onto the $TiO_2$ sample, leads to the formation of several adsorbed $NO_X$ species with absorption bands between 1100 and 2000 $cm^{-1}$. After 1 min of adsorption, strong

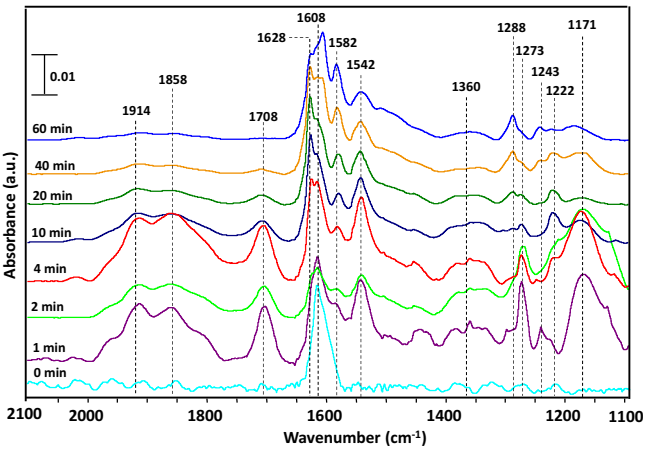


**Fig. 3.** *In-situ* trans-FTIR spectra of $TiO_2$ sample exposed to 25 Pa of $NO_2$ (1%/He) under dark condition at 296 K.

**Table 1**
Vibration assignments of adsorbed species produced during $NO_2$ adsorption on $TiO_2$ at 296 K.

| Adsorbed species | Wavenumber ($cm^{-1}$) | |
|---|---|---|
| | In this work | In literature |
| $N_2O_4$ | 1708, 1360, 1273 | 1710, 1350–1370, 1270–1265 [17,18] |
| $NO^+$ | 1914, 1858 | 1910–1890, 1840–1860 [17,28] |
| $NO_2^-$ | 1222 | 1225–1202 [18] |
| monodentate $NO_3^-$ | 1542 & 1243 | 1500–1600 [16,17] |
| bidentate $NO_3^-$ | 1608, 1582, 1288 | 1585–1605, 1280–1292 [25,26] |
| bridged $NO_3^-$ | 1628, 1171 | 1624–1590, 1200–1150 [27] |

absorption bands of $\nu$(NO) are observed at 1708 and 1273 $cm^{-1}$ with a weak $\nu$(NO) band at 1360 $cm^{-1}$. These bands are assigned to the adsorbed $N_2O_4$ species [17,18]. In parallel, two well resolved $\nu$(NO) bands attributed to monodentate nitrate (m-$NO_3^-$) species are observed at 1542 and 1243 $cm^{-1}$ [16,17]. Meanwhile, $\nu$(NO) absorption bands are observed at 1608, 1582, and 1288 $cm^{-1}$. These bands are ascribed to the bidentate nitrate (b-$NO_3^-$) species on $TiO_2$ surface [25,26]. In addition, two well resolved bands at 1628 and 1171 $cm^{-1}$ are observed. These bands are assigned to the bridged nitrate species [27]. Notably, the intensities of the bands at 1542 and 1243 $cm^{-1}$ (m-$NO_3^-$) and 1628 and 1171 $cm^{-1}$ (bridged $NO_3^-$) decrease with increasing adsorption time. More importantly, after 20 min of adsorption, these bands disappear and the intensities of the bands at 1608, 1582 and 1288 $cm^{-1}$ corresponding to b-$NO_3^-$ species increase as adsorption progress. Thus, it can be suggested that, bridged and m-$NO_3^-$ species are formed as intermediate species on $TiO_2$ surface, which are evidently converted into strongly adsorbed b-$NO_3^-$ species.

In literature, Ramis et al. [16] reported that, on activated $TiO_2$ (723 K), the molecularly adsorbed $NO_2$ shows two well resolved characteristic bands at 1617 and 1320 $cm^{-1}$. Interestingly, as reported in Fig. 3, these two bands are not observed. Therefore, it can be suggested that, on oxidized $TiO_2$ surface, at room temperature, as soon as $NO_2$ molecules adsorb, they get dimerized into strongly adsorbed $N_2O_4$ [18]. Meanwhile, along with $N_2O_4$ species, weak broad $\nu$(NO) bands at 1914 $cm^{-1}$ and at 1858 $cm^{-1}$ are also observed, and these bands disappear after 20 min of adsorption. These bands can be assigned to the adsorbed $NO^+$ species on $TiO_2$ surface [28,17]. Similarly, after 4 min of adsorption, a weak $\nu$(NO) band at 1222 $cm^{-1}$ is observed, and it disappears after 40 min of adsorption. This band can be assigned to the weakly adsorbed $NO_2^-$ species on $TiO_2$ surface [18].

It is worth to mention that the adsorbed $N_2O_3$ species on $TiO_2$ surface exhibit absorption bands between 1930 and 1880 $cm^{-1}$ [29], therefore it is very difficult to differentiate between the adsorbed $N_2O_3$ and the adsorbed $NO^+$ species on $TiO_2$ surface. However, Mikhaylov et al. [30] observed $N_2O_3$ species on $TiO_2$ surface only during NO and $O_2$ adsorption studies by the reaction between NO and $NO_2$ species on $TiO_2$ surface and also suggested that it is hard to identify the $N_2O_3$ species during $NO_2$ adsorption experiments. Ito et al. [31] suggested that during NO adsorption, $N_2O_3$ species exist in equilibrium with $NO_2^-$ and $NO^+$ species on $CeO_2$ surface as denoted in Eq. (5). In addition, Sentürk et al. [32] demonstrated $NO_2$ adsorption on $TiO_2/Al_2O_3$ binary mixture and suggested that $NO^+$ and $NO_2^-$ species are produced on the surface from $N_2O_3$ species as reported in Eq. (5). Therefore, it can be proposed that the existence of $N_2O_3$ could be correlated to the formation on $NO^+$ species on $TiO_2$ surface. Moreover, the consumption of $NO^+$ and $NO_2^-$ decreases the $N_2O_3$ concentration on $TiO_2$ surface at room temperature.

$$N_2O_{3(ads)} \leftrightarrow NO^+ + NO^-_{2(ads)} \quad (5)$$

### 3.3. $NO_2$ adsorption mechanism proposal based on surface analysis

The integration of characteristic absorption bands of adsorbed species leads to follow their individual evolutions as a function of time. For all species, the normalized absorbance is calculated by considering their individual maximum absorbance as 1. The normalized absorbances of primarily produced species $N_2O_4$ is reported in Fig. 4(a) and $NO^+$ and m-$NO_3^-$ species are reported in Fig. 4(b). Similarly, the normalized absorbances the intermediate species $NO_2^-$ and the strongly adsorbed b-$NO_3^-$ species are reported in Fig. 4(c). The $N_2O_4$ absorbance is followed through $\nu$(NO) stretching band at 1708 $cm^{-1}$, and the adsorbed $NO^+$ is followed through $\nu$(NO) band at 1914 $cm^{-1}$. The m-$NO_3^-$ is followed through $\nu$(NO) band at 1542 $cm^{-1}$, and the b-$NO_3^-$ is followed through $\nu$(NO) band at 1582 $cm^{-1}$. The $NO_2^-$ is followed through $\nu$(NO) band at 1222 $cm^{-1}$.

As can be seen in Fig. 4(a), the absorbance of $N_2O_4$ reaches maximum within 3 min, then steeply decreases to zero within 70 min of adsorption. Meanwhile, as reported in Fig. 4(b), the absorbance of $NO^+$ species increases and reaches maximum at 8 min, then decreases with increasing the adsorption time. The $NO^+$ species on $TiO_2$ surface is produced by intramolecular disproportionation reaction in $N_2O_4$ species at room temperature. The temporal profiles of $N_2O_4$ and $NO^+$ species show that they are converted into other species along adsorption experiment. The identification of $NO^+$ species on $TiO_2$ surface and subsequent conversion are coherent with the mechanism previously suggested by Sivachandiran et al. [15]. Our observations confirm this hypothesis.

Several experimental [33,34] and numerical studies [35–37] revealed the symmetric $O_2N$-$NO_2$ and asymmetric ONO-$NO_2$ isomers of $N_2O_4$. Fateley et al. [38] first reported the asymmetric isomer of $N_2O_4$ and demonstrated that it converts into an ion-pair of $NO^+NO_3^-$ at ambient temperature. Colussi et al. [39] estimated the heat of formation of ONO-$NO_2$ isomer from experiment to be $6.7 \pm 1$ kcal/mol which is only 4.5 kcal/mol less than the symmetry $O_2N$-$NO_2$ isomer. Givan et al. [33] evidenced that, using FTIR and Raman spectroscopy techniques, in spite of the fact that ONO-$NO_2$ is less stable, it is the main source of nitrosonium nitrate, *i.e.* $NO^+NO_3^-$ formation on copper substrate. Therefore, it can be suggested that on $TiO_2$ surface the $N_2O_4$ is adsorbed in the asymmetric form and produces $NO^+$ and $NO_3^-$ on $TiO_2$ surface. The $N_2O_4$ formation on $TiO_2$ surface and subsequent $NO^+$ formation on $TiO_2$ lattice

and m-$NO_3^-$ species production are summarized in Eq. (6) and Eq. (7).

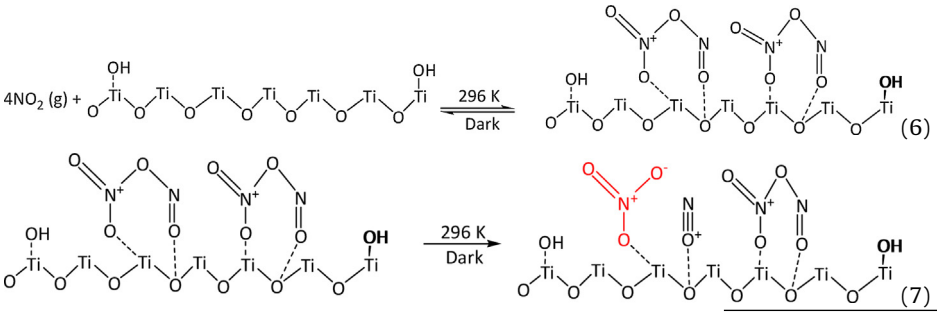


As reported in Fig. 4(b), m-$NO_3^-$ reaches maximum within 20 min, then gradually decreases with time. Thus, the decrease in intensity of m-$NO_3^-$ species shows that it is slowly converted into other species. We suggest that this species is converted into the strongly adsorbed b-$NO_3^-$ species, since this is the only species observed beyond 70 min of adsorption. This hypothesis is further praised by the increase in intensity of the strongly adsorbed b-$NO_3^-$ species as reported in Fig. 4(c). Moreover, the decrease in intensity of m-$NO_3^-$ is in accordance with the results reported by Sivachandiran et al. [15] based on gas phase analysis carried out at the reactor downstream. Indeed, it is possible to correlate the amount of $NO_2$ desorbed during TPD as a first peak to weakly adsorbed m-$NO_3^-$ species. Therefore, it can be concluded that, the m-$NO_3^-$ species are produced by the intramolecular disproportionation reaction from $N_2O_4$ species. Meanwhile, the relatively less stable $NO^+$ species adsorbed on $TiO_2$ surface reacts with the lattice $O^{2-}$ and produces $NO_2^-$ species. The m-$NO_3^-$ slow conversion and $NO_2^-$ species production can be summarized as follows:

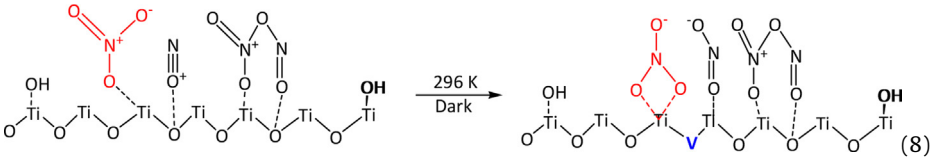


As reported in Fig. 4(c), similarly to m-$NO_3^-$ species, $NO_2^-$ reaches maximum at 20 min, then steeply decreases to zero within 70 min of adsorption. It can be suggested that the $NO_2^-$ species reacts with the adsorbed ONO-$NO_2$ and produces the strongly adsorbed b-$NO_3^-$ species as reported in Eq. (9). The $NO_2^-$ formation rate on $TiO_2$ surface is lower than the $NO^+$ and ONO-$NO_2$ formation rates, subsequently, it can be suggested that, $NO_2^-$ is produced as an intermediate species. As demonstrated by Apostolescu et al. [40] on $Al_2O_3$ surface, and as suggested by Sivachandiran et al. [15], and Mikhaylov et al. [30] on $TiO_2$ surface, it can be concluded that $NO_2^-$ is produced from $NO^+$ species. At room temperature, $NO^+$ is relatively unstable therefore, it may react with $O^{2-}$ on $TiO_2$ surface lattice leading to $NO_2^-$ species [40] and $Ti^{3+}$ sites on $TiO_2$ surface [41].

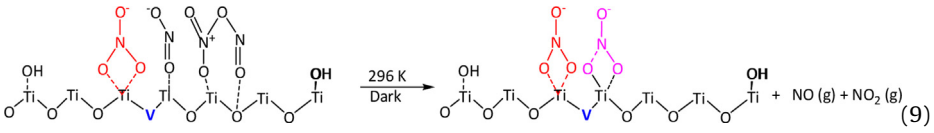


These findings give the possibility to complete and detail the mechanisms reported by Sivachandiran et al. [15]. The detailed complete global $NO_2$ adsorption equation can be written by summing up Eq. (6) to Eq. (9) as denoted in Eq. (10).

$$4NO_{2(ads)} + O^{2-}(TiO_{2\ \text{surface lattice}}) \overset{296K(dark)}{\leftrightarrow} 2b - NO^-_{3(ads)} + NO_{(g)} + NO_{2(g)} \quad (10)$$

In Eq. (8) and Eq. (9), "[V]" represents the lattice vacancy generated by the consumption of $O^{2-}$ by $NO^+$ species at 296 K. As denoted in Eq. (8), NO and $NO_2$ have not been observed in the gas phase using *in-situ* trans-FTIR. Although NO possess a strong polarization, it is a linear molecule with low extinction coefficient, thus, it is not observed in the gas phase under our experimental conditions. It can be suggested the as soon as $NO_2$ released into the gas phase, it could get dimerized on $TiO_2$ surface with another $NO_2$ molecule released in similar reaction as reported in Eq. (10). However, as abovementioned, gas phase monitoring reported by Sivachandiran et al. [15] interestingly complements the trans-FTIR results.

### 3.4. Assessment of $NO_2$ adsorption mechanism for various partial pressures

The proposed $NO_2$ adsorption mechanism on $TiO_2$ has been assessed for two different $NO_2$ partial pressures: 25 and 100 Pa. The temporal evolutions of adsorbed species on $TiO_2$ surface are discussed in the following.

#### 3.4.1. Formation of $N_2O_4$

Fig. 5 shows the evolution of adsorbed $N_2O_4$ species on $TiO_2$ surface as a function of time. For each investigated partial pressure the adsorbed $N_2O_4$ species have been observed as soon as $NO_2$ is introduced into the reactor. Therefore, it can be concluded that the $N_2O_4$ formation process on $TiO_2$ surface does not depend on $NO_2$ partial pressure. However, as can be seen in Fig. 5, the temporal evolution of $N_2O_4$ varies with $NO_2$ partial pressures. It can be expected that the increase in $NO_2$ partial pressure could increase the multilayer adsorption of $N_2O_4$ on $TiO_2$ surface. Nevertheless, the time required to reach the maximum of $N_2O_4$ on $TiO_2$ surface increases with increasing $NO_2$ partial pressure. Unlike 25 Pa, for 100 Pa partial pressures, the maximum is reached after 25 min adsorption, and then absorbance gradually decreases with time. This finding suggests the fact that, the increase in $NO_2$ partial pressure favors $N_2O_4$ conversion into m-$NO_3^-$ and $NO^+$ species on $TiO_2$ surface as reported in Eq. (6). Moreover, for 100 Pa, even after 70 min of adsorption, more than 70% of adsorbed $N_2O_4$ species remain

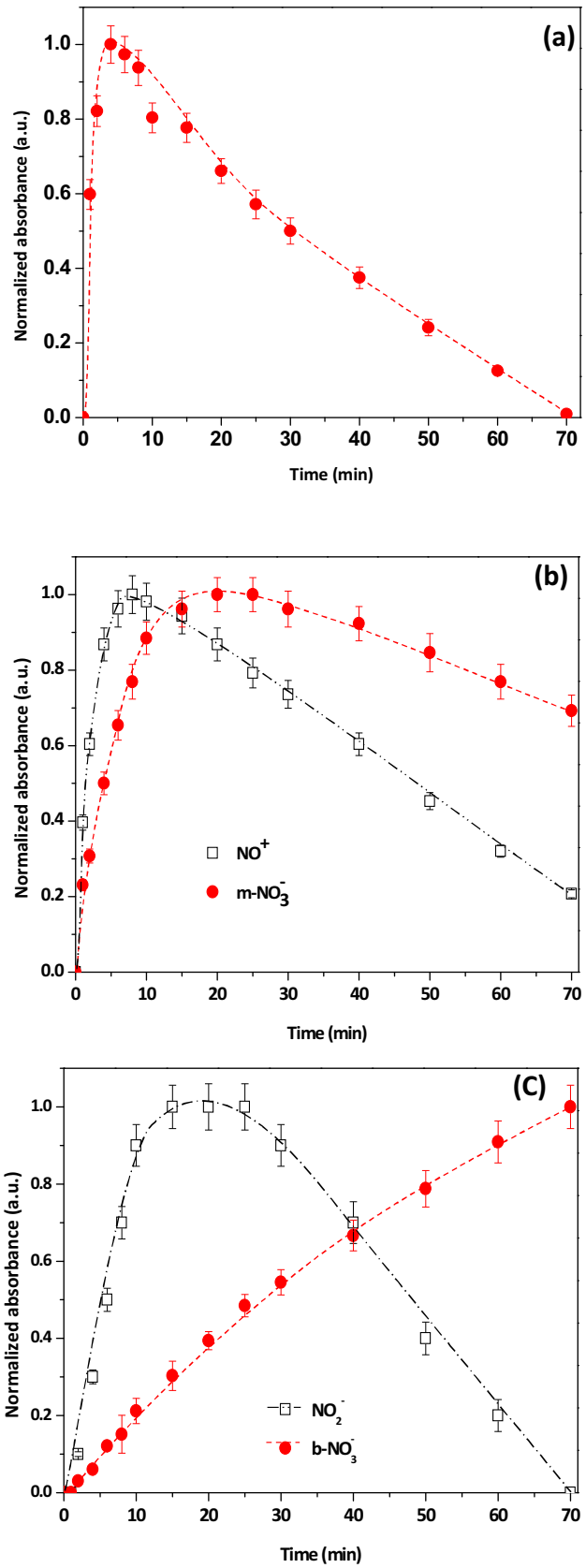


**Fig. 4.** Evolution of adsorbed species on $TiO_2$ surface during $NO_2$ adsorption. $NO_2$ adsorption is carried out at 296 K and under 25 Pa of $NO_2$ partial pressure. Normalized absorbances of adsorbed (a) $N_2O_4$, (b) $NO^+$ and m-$NO_3^-$, and (c) $NO_2^-$ and b-$NO_3^-$ species on $TiO_2$ as a function of time.

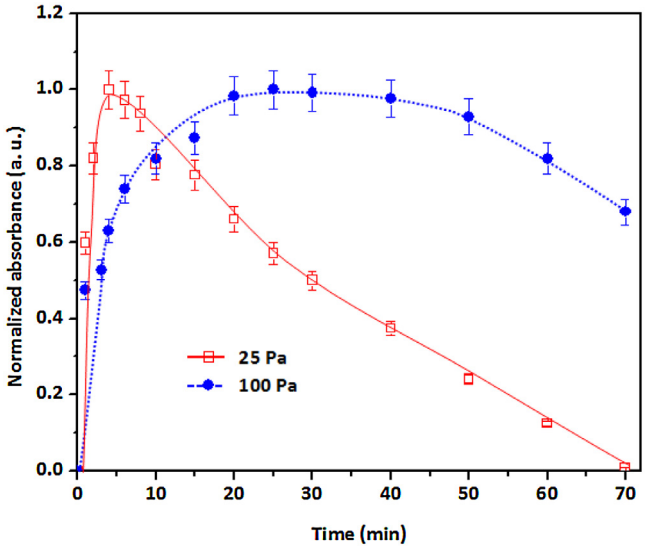


**Fig. 5.** Temporal evolution of normalized absorbance of adsorbed $N_2O_4$ species on $TiO_2$ surface, for partial pressures 25 and 100 Pa, as a function of time.

on $TiO_2$ surface. This observation implies the fact that increase in $NO_2$ partial pressure increases the concentration of adsorbed $N_2O_4$ species and are not completely converted into other adsorbed species. These suggestions could be confirmed by monitoring the evolution of m-$NO_3^-$ and $NO^+$ on $TiO_2$ surface for various $NO_2$ partial pressures.

### 3.4.2. *Intramolecular disproportionation reaction: formation of m-$NO_3^-$ and $NO^+$ species*

Fig. 6 reports the normalized absorbances of (a) m-$NO_3^-$ and (b) $NO^+$ species produced by the intramolecular disproportionation reaction in $N_2O_4$ species as a function of time for 25 and 100 Pa. It is worth to mention that for each investigated $NO_2$ pressure, the temporal profiles of m-$NO_3^-$ and $NO^+$ follow the same pattern.

As reported in Fig. 6(a), unlike $N_2O_4$ (Fig. 5) for both 25 and 100 Pa partial pressure the maxima of m-$NO_3^-$ are reached at 20 min. Indeed, as adsorption progresses, for 25 Pa pressure the m-$NO_3^-$ species concentration gradually decreases and about 70% remain even after 70 min, whereas, for 100 Pa it rapidly decreases with time and only about 10% remain after 70 min of adsorption. As suggested in *section 3.3*, the decrease in m-$NO_3^-$ coverage could be correlated to the formation of b-$NO_3^-$. As reported by Hadjiivanov et al. [18], even though the m-$NO_3^-$ species are produced from the adsorption of $N_2O_4$ on β-Lewis sites, *i.e.* $Ti^{4+}$ sites with one oxygen vacancy, the relatively less stable m-$NO_3^-$ has been converted into stable b-$NO_3^-$ species. Indeed, it can be suggested that the amount of m-$NO_3^-$ is mainly influenced by the first intramolecular disproportionation reaction and free adsorption sites on $TiO_2$ surface. This finding suggests the fact that the increase in $NO_2$ partial pressure favors the rate of m-$NO_3^-$ conversion into b-$NO_3^-$ species on $TiO_2$ surface.

As reported in Fig. 6(b), unlike m-$NO_3^-$ species, the time required to reach maximum coverage of $NO^+$ on $TiO_2$ surface increases with increasing the $NO_2$ partial pressure. Nevertheless, the rate of $NO^+$ conversion decreases with increasing the $NO_2$ partial pressure. For instance, for 25 Pa the maximum $NO^+$ concentration is reached at 5 min, whereas for 100 Pa the maximum reaches at 20 min. This finding, similarly to $N_2O_4$ formation, emphasizes the fact that the increase in $NO_2$ partial pressure increases the formation and conversion of $NO^+$ on $TiO_2$ surface for the first few minutes of adsorption. And thereafter, all these reactions are mainly dependent on the available free adsorption sites on

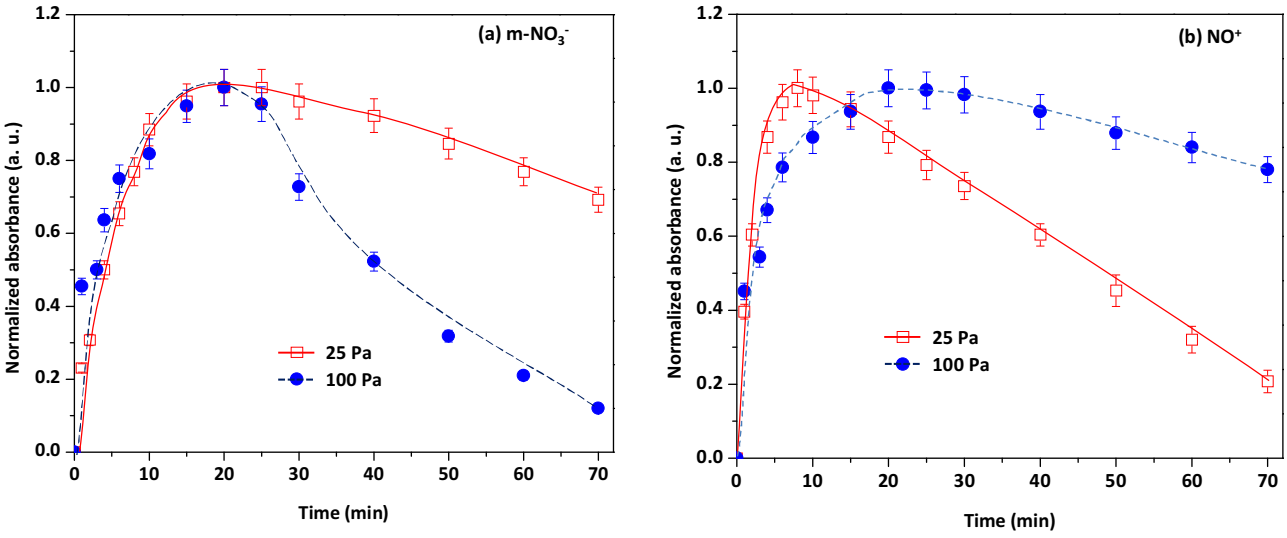


**Fig. 6.** Temporal evolution of normalized absorbances of (a) m-$NO_3^-$ and (b) $NO^+$ species for various partial pressures as a function of time.

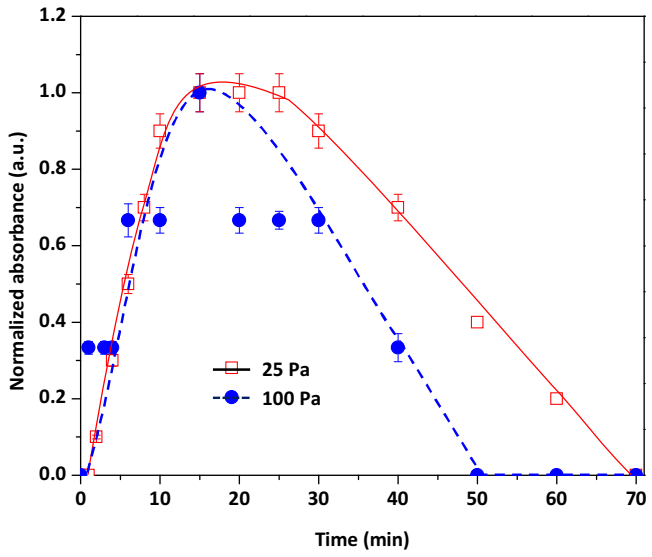


**Fig. 7.** Temporal evolution of normalized absorbance of $NO_2^-$ produced on $TiO_2$ surface for 25 and 100 Pa partial pressures as a function of time. $NO_2$ was introduced at room temperature and under dark condition.

$TiO_2$ surface. Although the adsorbed $NO^+$ species are relatively less stable on $TiO_2$ surface, for 100 Pa pressure, after 70 min adsorption, more than 80% remain on the surface. The existence of $NO^+$ can be ascribed to the formation of $N_2O_3$ by reacting with $NO_2^-$ on $TiO_2$ surface as reported in Eq. (5). This finding highlights the fact that $NO^+$ conversion into $NO_2^-$ is dependent on the surface coverage of m-$NO_3^-$ and b-$NO_3^-$ species, under dark condition.

### 3.4.3. Formation of $NO_2^-$: consumption of $TiO_2$ surface lattice oxygen ($O^{2-}$)

As discussed in *section 3.3*, the evolution of $NO_2^-$ species is followed as a function of time for each $NO_2$ partial pressure and reported in Fig. 7. The intermediate $NO_2^-$ is produced by the reaction between $NO^+$ and $TiO_2$ lattice oxygen ($O^{2-}$).

As can be seen in Fig. 7, similarly to m-$NO_3^-$ and $NO^+$ (Fig. 6), the coverage of $NO_2^-$ also varies according to the $NO_2$ partial pressure. For both 25 and 100 Pa partial pressure, the maxima are reached at 15 min. As reported in Eq. (8), though the $NO_2^-$ is produced form the adsorbed $NO^+$ and/or $N_2O_3$ species, the rate of $NO_2^-$ formation is not only dependent on $NO^+$ but also controlled by the intermolecular disproportionation reaction as reported in Eq. (12). As noticed in Fig. 7, after reaching the maximum coverage, for 100 Pa $NO_2$ partial pressure, the $NO_2^-$ concentration decreases faster than that of 25 Pa, and it reaches zero after 50 min of adsorption. Interestingly, as reported in Fig. 6(b), at 50 min of adsorption, the $NO^+$ coverage is about 90%. This finding emphasizes the fact that $NO^+$ conversion is not dependent on the $NO_2^-$ coverage on $TiO_2$ surface. Furthermore, as denoted in Eq. (8) and Eq. (11), it can be suggested that the rate of $NO^+$ conversion, *i.e.* the reaction between $NO^+$ and the lattice oxygen ($O^{2-}$) is much slower than the $NO_2^-$ conversion into b-$NO_3^-$ species.

$$NO^+_{(ads)} \leftrightarrow O^{2-}_{(surface\ lattice)} \overset{slow}{\leftrightarrow} NO^-_{2\ (ads)} \quad (11)$$

$$NO^-_{2\ (ads)} \leftrightarrow N_2O_{4\ (ads)} \overset{fast}{\leftrightarrow} b - NO^-_{3\ (ads)} + NO_{(gas)} + NO_{2(gas)} \quad (12)$$

### 3.4.4. Intermolecular disproportionation reaction: formation of b-$NO_3^-$

As reported in Fig. 3, it is evidenced that the b-$NO_3$- are the strongly adsorbed species on $TiO_2$ surface produced through intermolecular disproportionation reaction between $NO_2^-$ and $N_2O_4$ species on $TiO_2$ surface. Therefore, it can be proposed that the increase in $NO_2$ partial pressure could presumably increase the rate of b-$NO_3^-$ formation on $TiO_2$ surface. The evolution of b-$NO_3^-$ absorbance for 25 and 100 Pa $NO_2$ partial pressure, as function of time, is reported in Fig. 8.

As can be noticed in Fig. 8, for 25 and 100 Pa, the b-$NO_3^-$ absorbances follow the same trend. However, as expected, the rate of b-$NO_3^-$ formation increases with increasing the $NO_2$ partial pressure. Indeed, for 25 Pa partial pressure, the b-$NO_3^-$ absorbance gradually increases until 70 min of adsorption. Whereas, for 100 Pa the maximum absorbance is reached at 50 min. Interestingly, for 100 Pa $NO_2$ partial pressure, as reported in Figs. 6(b) and 7, after 50 min of adsorption the coverage of m-$NO_3^-$ and $NO_2^-$ reach 10% and zero, respectively. Therefore, there is no further intermolecular disproportionation reaction to produce b-$NO_3^-$ species. This finding shows that, the b-$NO_3^-$ species are produced by intermolecular disproportionation reaction and slow conversion of

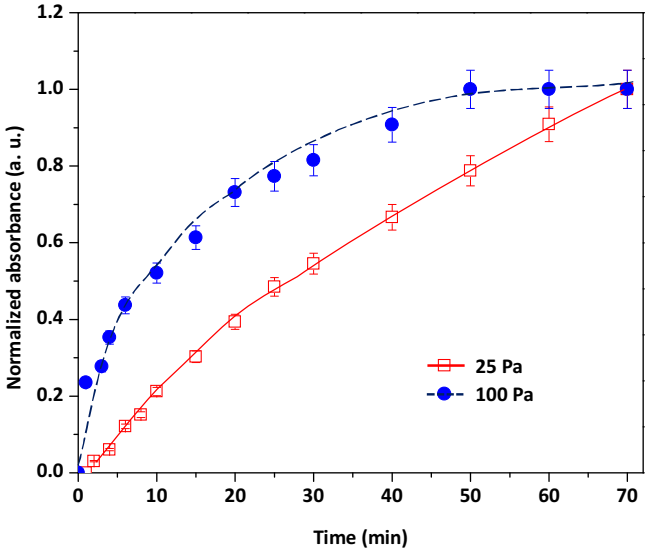


**Fig. 8.** Temporal evolution of normalized absorbance of b-$NO_3^-$ produced on $TiO_2$ for various $NO_2$ partial pressures as a function of time.

m-$NO_3^-$ species. Moreover, the rate of the reaction is dependent on $NO_2$ partial pressure and available free sites on $TiO_2$ surface.

As reviewed by Roy and Baiker [42], the storage of nitrate species on supports, *i.e.* metal oxide or mixture of metal oxides, is the main step directly linked with $NO_X$ reduction to $N_2$. As reported by Sivachandiran et al. [15], under a constant operating condition, an increase in $NO_2$ concentration decreases the $NO_2$ storage capacity. By taking into account the species monitored using gas phase FTIR, at the reactor downstream, it was suggested that the strongly adsorbed $NO_3^-$ species decreases the $NO_2$ adsorption/storage on $TiO_2$ surface. In this study using trans-FTIR, it is evidenced that the strongly adsorbed b-$NO_3^-$ species prevents the intra and intermolecular disproportionation reactions. As a result the adsorbed b-$NO_3^-$ species poisons the $TiO_2$ surface toward $NO_2$ adsorption and decreases the $NO_X$ storage capacity.

## 4. Conclusions

At 296 K, under dark condition, 25 and 100 Pa of $NO_2$ in He are introduced, and the adsorbed species on $TiO_2$ surface are followed using *in-situ* trans-FTIR spectroscopy, as a function of time. The main conclusions of this study are summarized below.

1. As soon as $NO_2$ is introduced onto $TiO_2$ surface, within less than 1 min, $NO_2$ species are dimerized to produce $N_2O_4$ on $TiO_2$ surface.
2. The species identified on $TiO_2$ surface are in accordance with the species proposed from the gas phase analysis performed at the reactor downstream as demonstrated by Sivachandiran et al. [15].
3. It was evidenced that, the first disproportionation reaction proceeds *via* an intramolecular disproportionation reaction, *i.e.* within one adsorbed $N_2O_4$ species, and produces weakly adsorbed monodentate nitrate (m-$NO_3^-$) species and highly reactive $NO^+$ species on $TiO_2$ surface. It was observed that, with time, the weakly adsorbed m-$NO_3^-$ species have been converted into strongly adsorbed bidentate nitrate (b-$NO_3^-$) species. Meanwhile, the highly active $NO^+$ species reacts with the lattice oxygen ($O^{2-}$) and produces $NO_2^-$ on $TiO_2$ surface.
4. The second disproportionation reaction is an intermolecular reaction, *i.e.* reaction between $N_2O_4$ and $NO_2^-$ species on $TiO_2$ surface. This reaction depends on the coverage of $NO_2^-$ and $N_2O_4$ species. It is proposed that, these two species should be in close vicinity to induce the disproportionation reaction and to produce NO in the gas phase and the strongly adsorbed b-$NO_3^-$ species on $TiO_2$ surface.
5. It was demonstrated that the rate of $N_2O_4$, m-$NO_3^-$ and $NO^+$ species formation are dependent on the $NO_2$ partial pressure.
6. The intermolecular disproportionation reaction, *i.e.* the reaction between $NO_2^-$ and $N_2O_4$ is faster than the relatively less stable $NO^+$ conversion into $NO_2^-$ species.
7. The $NO_2$ adsorption mechanism proposed based on gas phase analysis performed at the reactor downstream [15] is confirmed and precisely followed by *in-situ* $TiO_2$ surface analyses.

## Acknowledgements

The authors greatly acknowledge the French National Research Agency (ANR) for its financial support. Experiments have been performed in the framework of the ANR Blanc-RAMPE project.

## References

[1] Environmental Health Perspectives. 116-8 2008 A338.
[2] United States Environmental Protection Agency (EPA): http://www2.epa.gov/isa/integrated-science-assessment-isa-nitrogen-dioxide-health-criteria.
[3] J.H. Seinfeld, S.N. Pandis, Atmospheric Chemistry and Physics: from Air Pollution to Climate Change, 2nd ed., John Wiley, New York, 2006.
[4] M. Shimokawabe, K. Itoh, N. Takezawa, Catal. Today 36 (1997) 65–70.
[5] M. Shimokawabe, A. Ohi, N. Takezawa, React. Kinet. Catal. Lett. 52 (1994) 393–397.
[6] D. Mei, Q. Ge, J.H. Kwak, D.H. Kim, J. Szanyi, C.H. Peden, J. Phys. Chem. C 112 (2008) 18050–18060.
[7] N. Takahashi, A. Suda, I. Hachisuka, M. Sugiura, H. Sobukawa, H. Shinjoh, Appl. Catal. B Environ. 72 (2007) 187–195.
[8] L. Li, Q. Shen, J. Cheng, Z. Hao, Catal. Today 158 (2010) 361–369.
[9] S.M. Andonova, G.S. Şentürk, E. Özensoy, J. Phys. Chem. C 114 (2010) 17003–17016.
[10] C. Morterra, G. Ghiotti, E. Garrone, E. Fisicaro, J. Chem. Soc. Faraday Trans. 1 (76) (1980) 2101–2113.
[11] J. Haubrich, R.G. Quiller, L. Benz, Z. Liu, C.M. Friend, Langmuir 26 (2010) 2445–2451.
[12] J.A. Rodriguez, T. Jirsak, G. Liu, J. Hrbek, J. Dvorak, A. Maiti, J. Am. Chem. Soc. 123 (2001) 9597–9605.
[13] J. Abad, O. Bohme, E. Roman, Langmuir 23 (2007) 7583–7586.
[14] A. Folli, S.B. Campbell, J.A. Anderson, D.E. Macphee, J. Photochem. Photobiol. A 220 (2011) 85–93.
[15] L. Sivachandiran, F. Thevenet, P. Gravejat, A. Rousseau, Appl. Catal. B Environ. 143 (2013) 196–204.
[16] G. Ramis, G. Busca, V. Lorenzelli, Appl. Catal. 64 (1990) 243–257.
[17] G. Ramis, G. Busca, F. Bregani, P. Forzatti, Appl. Catal. 64 (1990) 259–278.
[18] K. Hadjiivanov, V. Bushev, M. Kantcheva, D. Klissurski, Langmuir 10 (1994) 464–471.
[19] J.S. Dalton, P.A. Janes, N.G. Jones, J.A. Nicholson, K.R. Hallam, G.C. Allen, Environ. Pollut. 120 (2002) 415–422.
[20] F. Arsac, D. Bianchi, J.M. Chovelon, C. Ferronato, J.M. Herrmann, J. Phys. Chem. A 110 (2006) 4202–4212.
[21] P.F. Rossi, G. Busca, V. Lorenzelli, O. Saur, J.C. Lavalley, Langmuir 3 (1987) 52–58.
[22] M.E. Maazawi, A.N. Finken, A.B. Nair, V.H. Grassian, J. Catal. 191 (2000) 138–146.
[23] C. Deiana, E. Fois, S. Coluccia, G. Martra, J. Phys. Chem. C 114 (2010) 21531–21538.
[24] G. Piazzesi, M. Elsener, O. Krocher, A. Wokaun, Appl. Catal. B Environ. 65 (2006) 169–174.
[25] K. Hadjiivanov, H. Knozinger, Phys. Chem. Chem. Phys. 2 (2000) 2803–2806.
[26] A.L. Goodman, E.T. Bernard, V.H. Grassian, J. Phys. Chem. A 105 (2001) 6443–6457.
[27] G.M. Underwood, T.M. Miller, V.H. Grassian, J. Phys. Chem. A 103 (1999) 6184–6190.
[28] R.V. Mikhaylov, A.A. Lisachenko, B.N. Shelimov, V.B. Kazansky, G. Martra, G. Alberto, S. Coluccia, J. Phys. Chem. C 113 (2009) 20381–20387.
[29] K. Hadjiivanov, Catal. Rev. Sci. Eng. 42 (2000) 71–144.
[30] R.V. Mikhaylov, A.A. Lisachenko, B.N. Shelimov, V.B. Kazansky, G. Martra, S. Coluccia, J. Phys. Chem. C 117 (2013) 10345–10352.
[31] E. Ito, Y.J. Mergler, B.E. Nieuwenhuys, H. van Bekkum, C.M. van den Bleek, Microporous Mater. 4 (1995) 455–465.
[32] G.S. Sentürk, E.I. Vovk, V.I. Zaikovskii, Z. Saya, A.M. Soylu, V.I. Bukhtiyarov, E. Ozensoy, Catal. Today 184 (2012) 54–71.
[33] A. Givan, A. Loewenschuss, J. Chem. Phys. 90 (1989) 6135.
[34] D.A. Pinnick, S.F. Agnew, B.I. Swanson, J. Phys. Chem. 96 (1992) 7092.

[35] W.G. Liu, W.A. Goddard, J. Am. Chem. Soc. 134 (2012) 12970–12978.
[36] M.L. McKee, J. Am. Chem. Soc. 117 (1995) 1629–1637.
[37] E.A. Pidko, P. Mignon, P. Geerlings, R.A. Schoonheydt, R.A. van Santen, J. Phys. Chem. C 112 (2008) 5510–5519.
[38] W.G. Fateley, H.A. Bent, B. Crawford, J. Chem. Phys. 31 (1959) 204.
[39] A.J. Colussi, M.A. Grela, J. Phys. Chem. 97 (1993) 3775.
[40] N. Apostolescu, T. Schröder, S. Kureti, Appl. Catal. B Environ. 51 (2004) 43–50.
[41] G.B. Hoflund, H.L. Yin, A.L. Grogan, D.A. Asbury, Langmuir 4 (1988) 346–350.
[42] S. Roy, A. Baiker, Chem. Rev. 109 (2009) 4054–4091.